Electronic Supplementary Material (ESI) for ChemComm.
This journal is © The Royal Society of Chemistry 2020

Supporting Information for:

Double Defective Groups Modified Nitrogen-Deficient Carbon Nitride with Bimetallic PtSn as Cocatalysts for Efficient Photocatalytic Hydrogen Evolution up to 765 nm

Shushu Huang, Yanxia Zhang, Chunfang Du* and Yiguo Su*

College of Chemistry and Chemical Engineering, Inner Mongolia University, Hohhot, Inner Mongolia 010021, P. R. China

1. Experimental section

1.1 Catalysts preparation

1.1.1 Preparation of nitrogen-deficient carbon nitride

Nitrogen-deficient carbon nitride was obtained by the traditional solid-state reaction. Briefly, 3 g urea was calcined at 550 ^{o}C for 3 h with the heating rate of 5 ^{o}C/min. And the cooling rate was also 5 ^{o}C/min. The obtained light yellow product was obtained after washing three times with deionized water and ethyl alcohol. The prepared nitrogen-deficient carbon nitride sample was named as D-g-C_3N_4.

1.1.2 Preparation of KSCN modified D-g-C_3N_4

In detail, 3 g potassium rhodanate (KSCN) and 1.5 g D-g-C_3N_4 were fully mixed in an agate mortar. Then the mixture was transferred into the corundum crucible and calcined in a tube furnace under nitrogen to 400 ^{o}C for 1 h, then at 500 ^{o}C for 30 min, both with a heating rate of 5 ^{o}C/min. The prepared product was washed repeatedly with water until residue of KSCN was removed and then dried at 60 ^{o}C. The obtained sample was named as KSCN-D-g-C_3N_4.

1.1.3 Preparation of defective carbon nitride

Defective carbon nitride was synthesized by treating KSCN-D-g-C_3N_4 with aqueous HCl. In brief, 30 mL HCl (12 mol/L) was added into a contained KSCN-D-g-C_3N_4 beaker with magnetic stirring for 15 h. Finally, milky product was obtained, which was washed three times with water and alcohol. And the prepared sample was named as CNx.

1.1.4 Preparation of PtSn/CNx

0.1 g CNx was dispersed into 80 mL deionized water with ultrasound treatment about 20 min. A certain amount of aqueous H_2PtCl_6 (10 mg/mL) and aqueous $SnCl_4$ (0.01 mmol/mL) were added with magnetic stirring for 10 min. 20 mL triethanolamine (TEOA) was added into the suspension to form a (TEOA)-H_2O solution (V/V = 20%). The suspension was evacuated several times to remove the air and ensure the reactor in a vacuum atmosphere before irradiation. The final product was collected after the H_2 evolution and washed three times using deionized water and ethyl alcohol and then dried in an oven at 60 ^{o}C. PtSn/CNx photocatalysts were synthesized with different molar ratios of Pt and Sn (3.5:0, 1.5:1, 2.5:1, 3.5:1 and 4.5:1), which were named as PS1-CNx, PS2-CNx, PS3-CNx, PS4-CNx and PS5-CNx. Additionally, the real molar ratios of Pt and Sn was measured by inductively coupled plasma atomic emission spectroscopy (ICP-AES), which was displayed in the following table.

Sample	Initial molar ratios	Measured molar ratios	Pt wt%	Sn wt%
PS2-CNx	1.5:1	0.28:1	1.53	3.35
PS3-CNx	2.5:1	0.70:1	3.61	3.19

PS4-CNx	3.5:1	1:1	4.86	3.02
PS5-CNx	4.5:1	1.48:1	7.78	3.25

1.2 Sample characterization

The wide-angle X-ray power diffraction (XRD) performing on a Rigaku DMAX2500 X-ray diffractometer with Cu Kα radiation was carried out in order to investigate the crystal phase structures. Scanning electron microscopy (SEM) was performed on a HITACHI S-4800 apparatus, which applied to investigate the morphologies of the obtained photocatalysts. The morphologies and lattice spacing of the as-prepared samples were recorded by transmission electron microscopy (TEM) using a FEI Tecnai G2 F20 S-TWIN field emission microscope apparatus with an acceleration voltage of 200 kV. Perkin Elmer UV/VS/NIR Lambda 750 s spectrometer was performed to measure the ultraviolet-visible DRS of the obtained products. X-ray Photoelectron Spectroscopy (XPS) analyses were performed on an ESCALab220i-XL with a monochromatic Al Kα and charge neutralizer. The C 1s peak at 284.6 eV was used for the referenced binding energy for samples. All calculations were performed with density functional theory, using the CASTEP program package. The kinetic energy cutoff is 571.4 eV, using the generalized gradient approximation (GGA) with the Perdew-Burke-Ernzerhof (PBE) to treat the models. Geometry optimization is carried out until the residual forces were smaller than 0.01 eV $Å^{-1}$, and the convergence threshold for self-consistent iteration was set at 1×10^{-6} eV. The photoluminescence (PL) and time-resolved fluorescence decay

spectra were measured on an Edinburgh Instruments FLS920 spectrofluorimeter equipped with both continuous and pulsed xenon lamps. The wavelength of excitation light for emission spectra and transient decays was 310 nm for all samples. The transient photocurrent response of the samples with light on/off cycles were carried out on the Metrohm Autolab (PGST AT302N) under white (neutral) light irradiation (LED 690 lm, [Na_2SO_4] = 0.2 M). Electrochemical impedance spectroscopy (EIS) measurements were performed to investigate the migration rate of charge carrier with the frequency from 0.1 Hz to 100 KHz. Na_2SO_4 aqueous solution (0.2 M, pH = 7) was served as the electrolyte. Mott-Schottky plots of carbon nitrogen were performed at the frequency of 1000 Hz in the dark. EPR spectra were performed using an ER200-SRC electron spin resonance spectrometer (Bruker, Germany) at 3186 G and 9056.895 MHz.

1.3 Photocatalytic hydrogen evolution

Photocatalytic hydrogen production activity was conducted in a quartz flask sealed system with a side window for irradiation. The light source was a 300 W xenon lamp with a 420 nm cutoff filter ($\lambda \geq 420$ nm). In experiment, 100 mg sample was dispersed in a mixture of 80 mL deionized water and 20 mL triethanolamine (TEOA) which served as a sacrificial agent. Bimetallic PtSn was deposited on the surface of the catalyst as cocatalyst and the solution was evacuated to drive away air in the reaction before illumination. The yield of H_2 production was investigated on an online gas chromatograph (GC-7920, TCD, Ar as the carrier).

The apparent quantum efficiency (AQE) was confirmed by using AQE (%) = (2 ×

Numbers of H_2/Numbers of incident photons) × 100. The light source used in experiment was a 300 W Xenon lamp with different wavelength filter. And the numbers of incident photons was determined by a calibrated Si photodiode.

The apparent quantum efficiency (AQE) was calculated by follow:

$$AQE = \frac{2 \times Numbers\ of\ H_2}{Numbers\ of\ incident\ photons} \times 100\%$$

$$= \frac{N_e}{N_p} \times 100\% = \frac{2 \times M \times N_A}{\frac{E_{total}}{E_{photon}}} \times 100\%$$

$$= \frac{2M \times N_A}{\frac{S \times P \times t}{h \times \frac{C}{\lambda}}} \times 100\% = \frac{2 \times M \times N_A \times h \times c}{S \times P \times t \times \lambda} \times 100\%$$

Where, M is the amount of H_2 molecules (mol), N_A is Avogadro constant (6.022×10^{23}/mol), h is the Plank constant (6.626×10^{-34} J S), c is the speed of light (3×10^{8} m/s), S is the irradiation area (cm^2), P is the intensity of irradiation light (W/cm^2), t is the photoreaction time (s), λ is the wavelength of the monochromatic light (m).

And the parameters of the irradiation light used in this work were presented in the following table. Meanwhile, the photoreaction time in this work is 3600 s.

Table S1 Parameters of the irradiation light.

Wavelength (nm)	Light intensity (mW/cm^2)	Time (s)	Irradiation area (cm^2)
420	19.4	3600	23.75
435	10.7		
450	10.2		

475	7.5		
500	10.2		
520	17.2		
600	15		
700	13.8		
765	11.2		

Fig. S1 XRD patterns of the obtained samples.

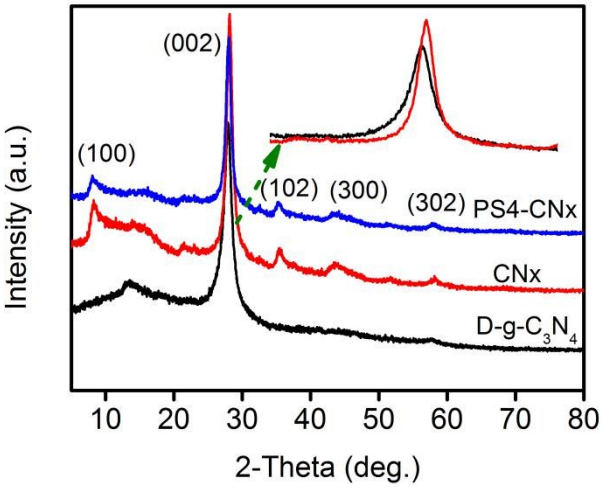

Clearly, two characteristic diffraction peaks located at 13.4 and 27.9° in the XRD pattern of D-g-C_3N_4, which belonged to (100) and (002) planes of graphitic carbon nitride, respectively.[1] Several additional diffraction peaks presented in CNx and the narrowed full width at half-maximum (FWHM) of the peak for CNx suggested the improved crystallinity of CNx in comparison to D-g-C_3N_4.[2,3] And, the additional peaks of CNx were assigned to the diffraction planes of carbon nitride according to previous report.[4]

Fig. S2 Enlarged XRD patterns of D-g-C_3N_4 and CNx.

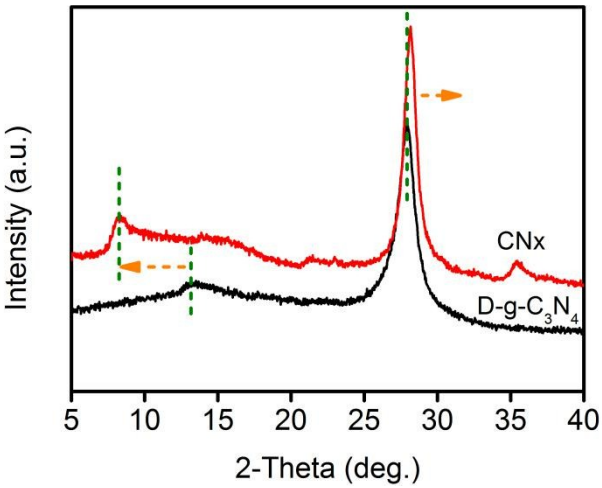

It is worth noting that the (100) plane of CNx shifted from 13.4° to 8.3° compared to D-g-C_3N_4, which was attributed to the more stretched in-plane structure.[5] Meanwhile, the (002) plane of CNx was slightly shifted to a higher angle than D-g-C_3N_4, indicating a decrease in the interlayer stacking distance.[6]

Fig. S3 SEM image of D-g-C_3N_4.

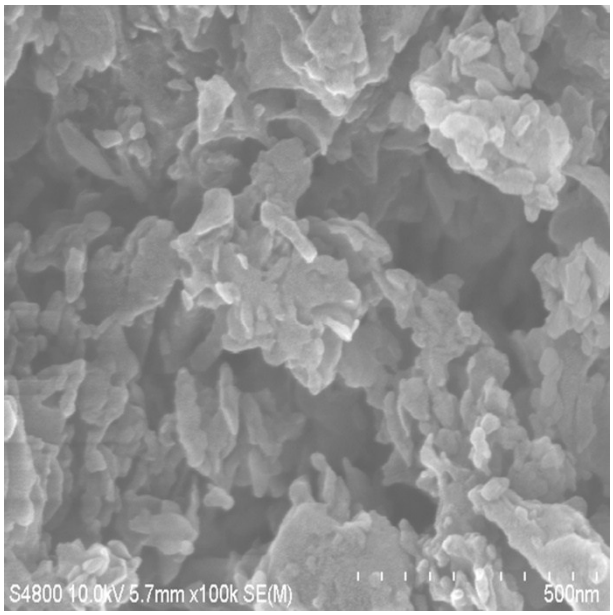

Fig. S4 HRTEM image of PS4-CNx sample

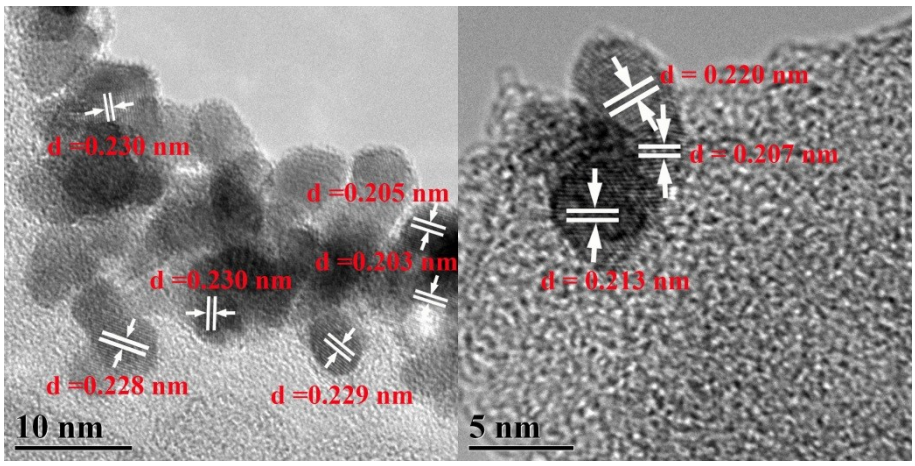

Fig. S5 XPS survey spectra of D-g-C_3N_4, CNx and PS4-CNx samples.

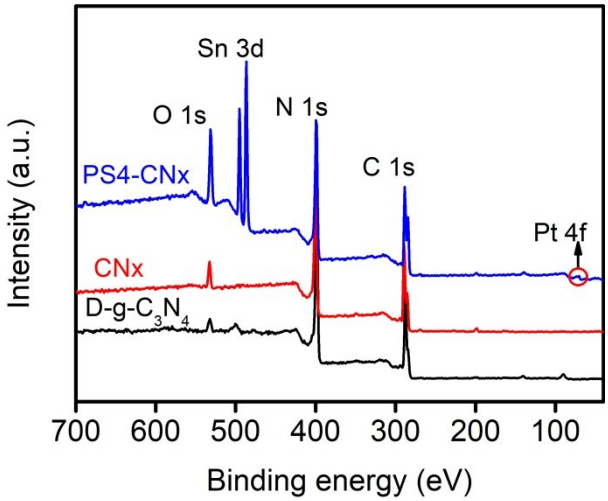

XPS survey spectra presented that C, N, O elements were co-existed in D-g-C_3N_4 and CNx samples. XPS survey spectrum of PS4-CNx demonstrated that Pt and Sn elements were successfully decorated on CNx surface.

Fig. S6 N 1s XPS spectra of D-g-C_3N_4 and KSCN-D-g-C_3N_4.

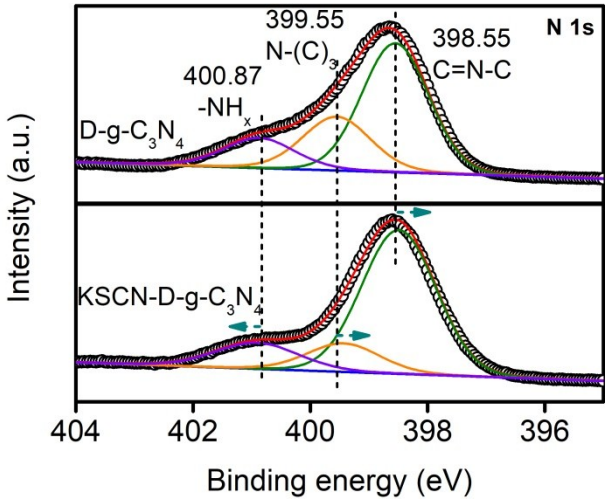

N 1s XPS spectrum of D-g-C_3N_4 illustrated that three peaks located at 398.55, 399.55 and 400.87 were ascribed to C=N-C, N-$(C)_3$ and –NH_x groups, respectively.[7] Moreover, the proportion of –NH_x group in KSCN-D-g-C_3N_4 was decreased to 15.0% from 15.8% in D-g-C_3N_4. Meanwhile, a slight shift of –NH_x to higher binding energy and little shift of C=N-C and N-$(C)_3$ to lower binding energy in KSCN-D-g-C_3N_4 sample further demonstrated that the formation of -C≡N group.[8]

Fig. S7 C 1s XPS spectra of CNx and PS4-CNx.

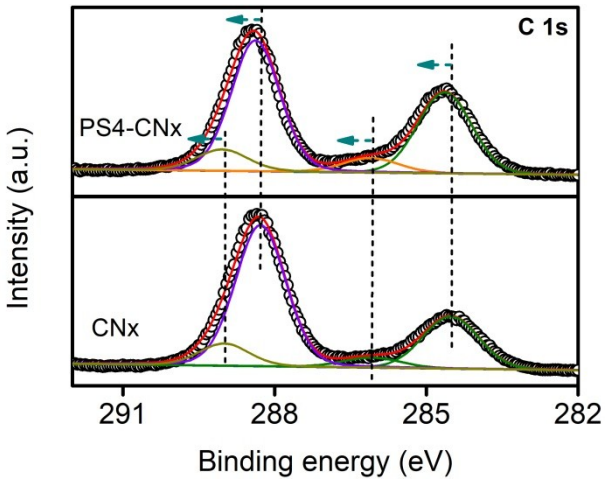

Fig. S8 N 1s XPS spectra of CNx and PS4-CNx.

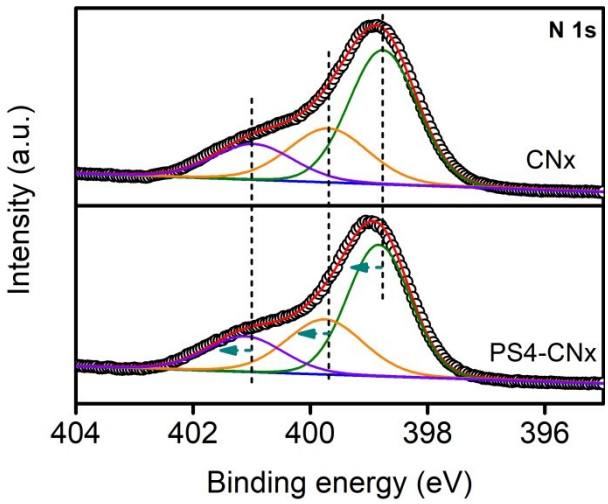

Fig.S9 Band gap energy of D-g-C_3N_4 and CNx.

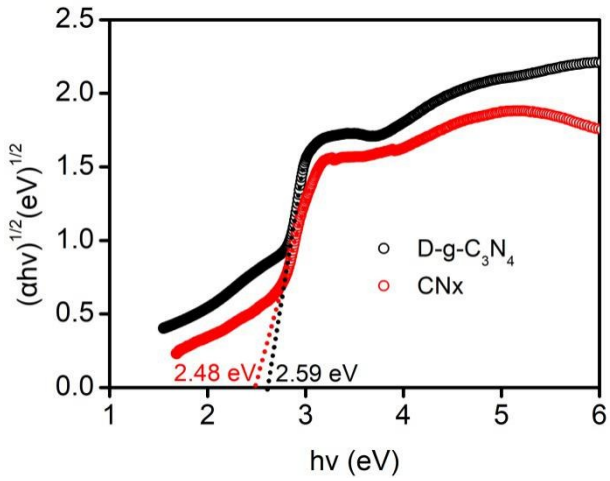

Fig. S10 Models and band structure of bulk g-C_3N_4 and carbon nitrogen with nitrogen vacancy.

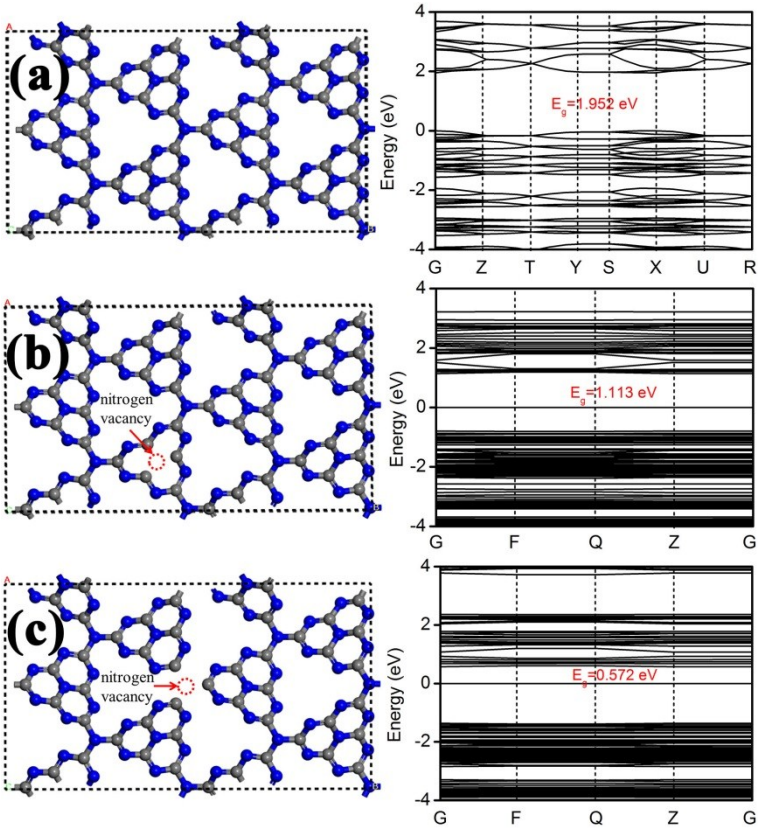

Fig. S11 Models and band structure of bulk g-C_3N_4 (a) and cyano group modified carbon nitrogen (b).

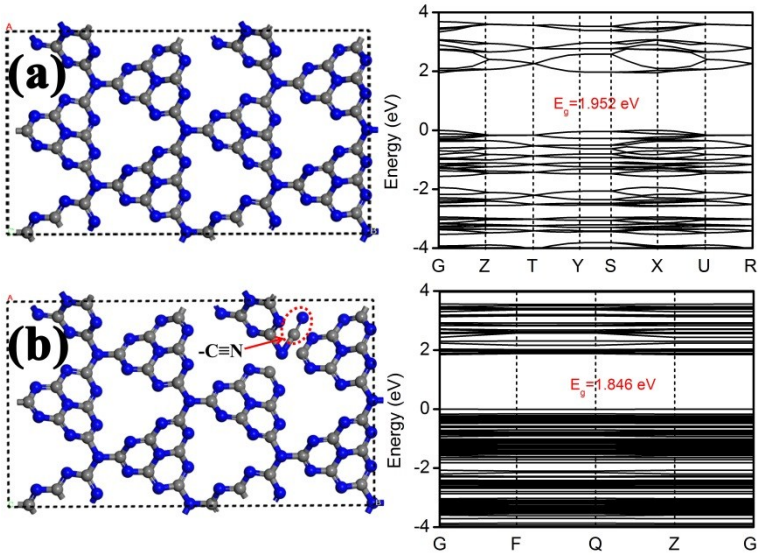

Fig. S12 Models and band structure of bulk g-C_3N_4 (a) and urea group modified carbon nitrogen (b).

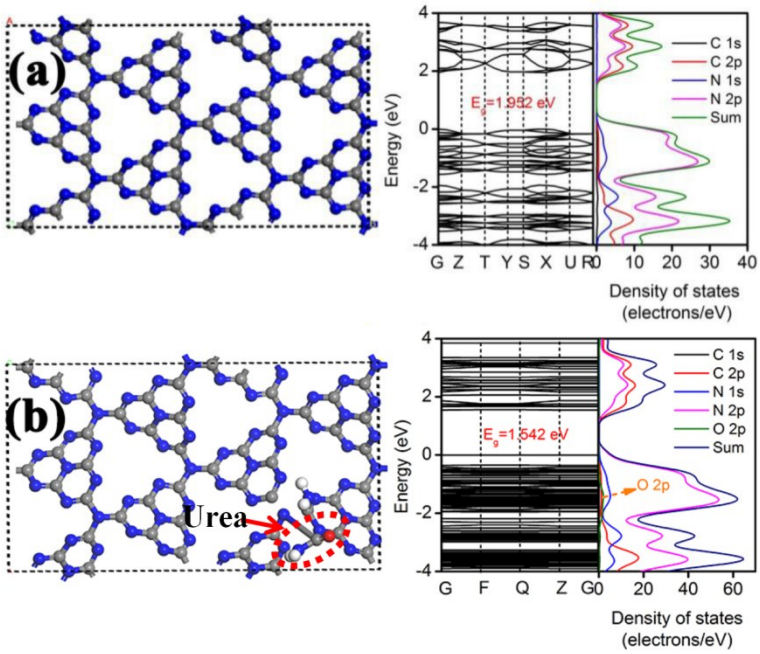

The results of DFT calculation indicated that band gap energy of carbon nitride can be narrowed by introducing nitrogen vacancy, cyano or urea groups, corresponding to the result of Fig. 3a. It is worth noting that the electron density of band structure for the modified carbon nitrogen was increased compared with g-C_3N_4, contributing to accelerating the transfer of photogenerated electrons and then promoting the photocatalytic performance. Additionally, O 2p was participated in the formation of band structure of urea group modified carbon nitride (Fig. S12b), also indicating that the band structure of carbon nitrogen can be regulated by defective group.

Fig. S13 Mott-Schottky plots of D-g-C_3N_4 and CNx.

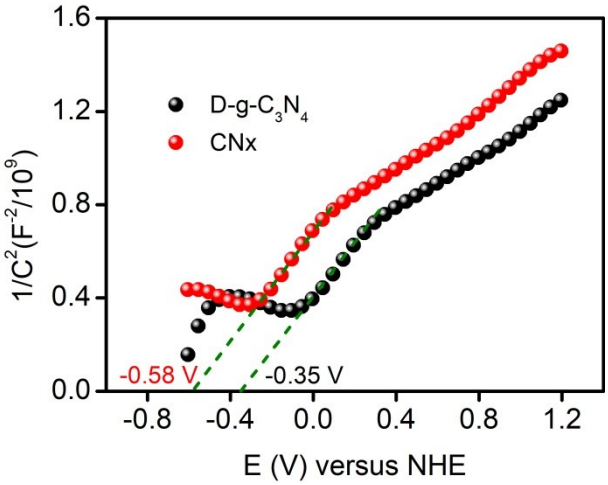

The Mott-Schottky analysis was carried out to determine the flat band potential (E_{fb}) and conduction band (CB) edges of the photocatalysts. The Schottky plots of carbon nitride owned a positive slope, which identified that the D-g-C_3N_4 and CNx were assigned to n-type semiconductors, coinciding with previously literature.[9] The flat band potentials (E_{fb}) of D-g-C_3N_4 and CNx were estimated using the extrapolation of the Mott-Schottky plot at the frequency of 1000 Hz. It was known that the conduction band potentials of n-type semiconductors were closed to the flat potential.[10] Hence, the conduction band potential of D-g-C_3N_4 and CNx was estimated to be -0.35 V and -0.58 V versus NHE.

Fig. S14 Electric structure of D-g-C_3N_4 and CNx.

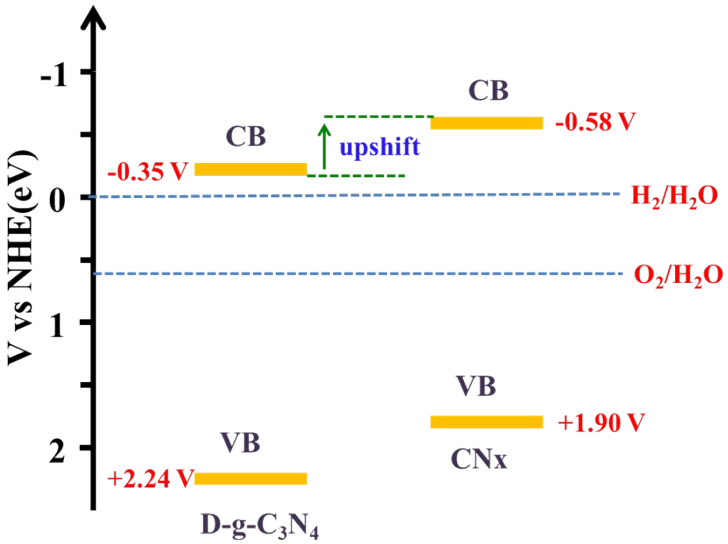

Fig. S15 Valence band XPS (VB-XPS) analysis of D-g-C_3N_4 and CNx.

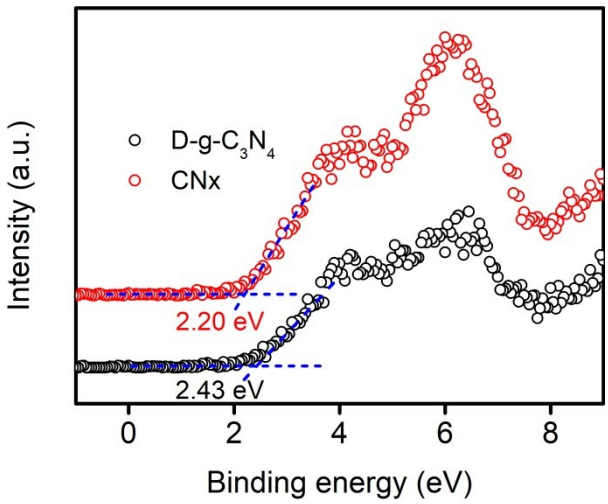

Fig. S16 UV-visible diffuse reflectance spectra of CNx and PS4-CNx.

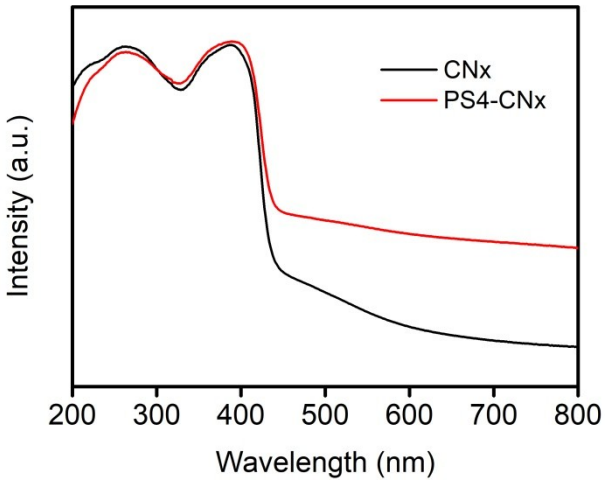

Fig. S17 N_2 adsorption/desorption isotherms of samples. Insert is the pore size distribution of D-g-C_3N_4 and CNx.

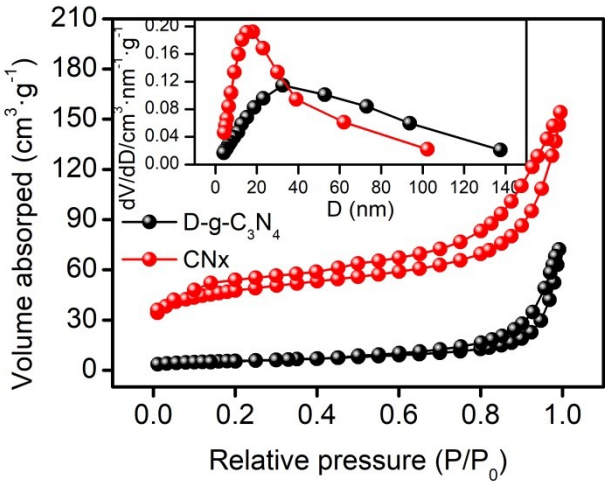

As is well-known that semiconductor photocatalyst owned a larger specific surface area always accompanied with more reactive sites.[11] Obviously, the N_2 adsorption-desorption isotherms presented a type IV character. And the surface area of CNx was 153.23 $m^2 \cdot g^{-1}$, which was about 7.8 times larger than that of D-g-C_3N_4 (19.52 $m^2 \cdot g^{-1}$), endowing more reactive sites on the CNx surface. Moreover, the higher pore-size distribution curve of CNx indicated more porous structure than D-g-C_3N_4, which might be beneficial to facilitating the diffusion of reactants and products, then leading to the improvement of phtocatalytic activity.[12]

Fig. S18 Photocatalytic H_2 evolution performance under visible light irradiation.

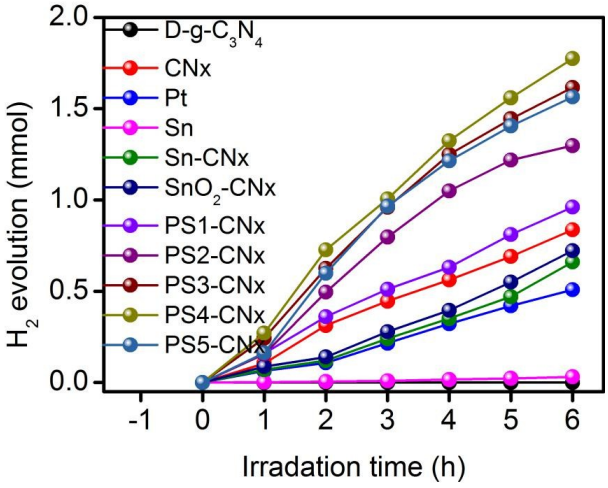

Fig. S19 Photocatalytic H_2 evolution performance under different single-wavelength irradiation.

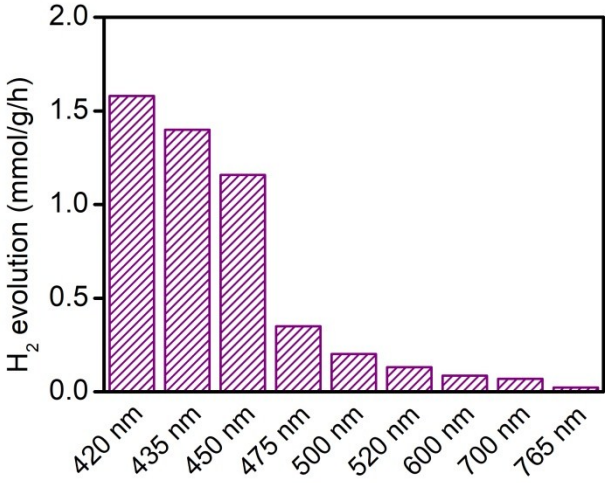

Table S2 Comparison of AQE of PS4-CNx with those of other catalysts reported in literature.

Entry	Catalysts	AQE (%)	Wavelength (nm)	ref
1	CNx-4	8.42	435	this work
2	C-PAN/g-C_3N_4	5.6	420	13
3	UM3	27.8	420±15	14
4	Monolayer O-g-C_3N_4	13.7	420	15
5	Mesoporous g-C_3N_4 nanomesh	5.1	420	16
6	quasi-honeycomb g-C_3N_4	6.27	400	17
7	g-C_3N_4 nanosheets	3.6	420	18
8	Pt/CNS	2.4	420	19
9	CdS/1.3%Ni_2P/g-C_3N_4	0.18	420	20
10	CNBN-3	2.02	420	21
11	C_3N_4/1%CBV^{2+}	3.81	420	22

12	UP10	5.72	420	23
13	HC-CN	6.17	420	24
14	DCN-3	17.25	420±10	25
15	PtAu-2/g-C_3N_4	0.45	420±10	26
16	CdS/Cu_7S_4/g-C_3N_4	4.4	420	27
17	$Bi_2O_2CO_3$/g-C_3N_4	7.14	420	28
18	Pd-Ag/g-C_3N_4	8.7	460	29
19	3-TC/CN	0.81	400	30
20	MC-3.2%	5.67	400±5	31
21	C-ZrO_2/g-C_3N_4/20 %Ni_2P	35.5	420	32
22	HDCN	16.2	420	8
23	C_3N_4/Fe_2O_3@FeP-60	38.8	420	33
24	CN-OA-m	57.0 (in NaCl solution)	420	34

25	CN-NaK	60.0 (in sea water)	420	3
26	2D/2D Co_3O_4/g-C_3N_4	53.6	405	35
27	2D/2D V_2O_5/g-C_3N_4	67.71	400	35
28	g-CN	50.7	405	36
29	Ni-MOF/g-C_3N_4	58.1	420	37

Fig. S20 Transient photocurrent response of PS4-CNx sample under the light at 765 nm irradiation.

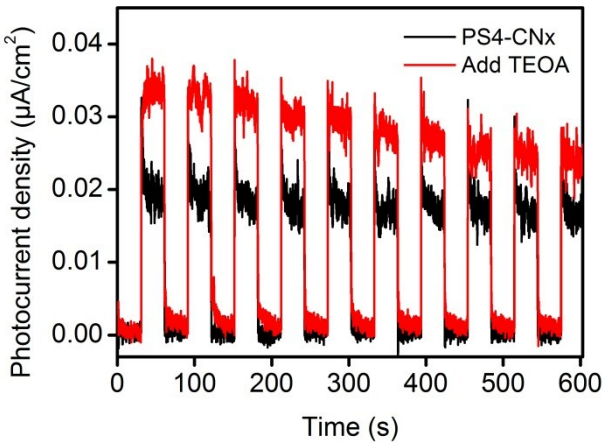

It could be clearly seen from the DFT calculation analysis (Fig. S10) that a midgap state was generated for carbon nitride containing nitrogen vacancy. According previously reported literature, nitrogen vacancy derived midgap states would accommodate more charge carriers excited by the photons at longer wavelengths.[38] The previous reports pointed out that the organics with unsaturated heteroatomic groups have an n electrons and p electrons. Electrons at n orbital can be exited to π* orbital by the light with a certain frequency, which is called the n→π* transition.[39] And the effective overlap of n orbital and p orbital in cyano groups would lead to a new absorption band of longer wavelength in carbon nitride photocatalyst.[40] Meanwhile, the O-containing groups also resulted in the formation of defect-related state below conduction band minimum (CBM) of carbon nitride, then forming an additional long wavelength absorption.[41] Additionally, the well planarized layers in crystalline carbon nitride also can bring out a wider absorption in UV-vis light spectra.[42] Hence, the modified carbon nitride catalysts in this work could absorb light up to 765 nm. The transient photocurrent response of PS4-CNx under the light at 765

nm irradiation (Fig. S20) declared that charge carriers could be generated with 765 nm light irradiation. Hence, the photogenerated electrons in the conduction band of PS4-CNx are able to reduce protons to H_2 molecules. Furthermore, the photocurrent density enhanced with addition of sacrificial reagents (TEOA), suggesting the boosted separation of photogenerated electron-hole pairs. It is considered that TEOA was oxidized by the photogenerated holes, improving the separation efficiency of photogenerated charge carriers.

Fig. S21 Photoluminescence (PL) spectra of the as-prepared samples.

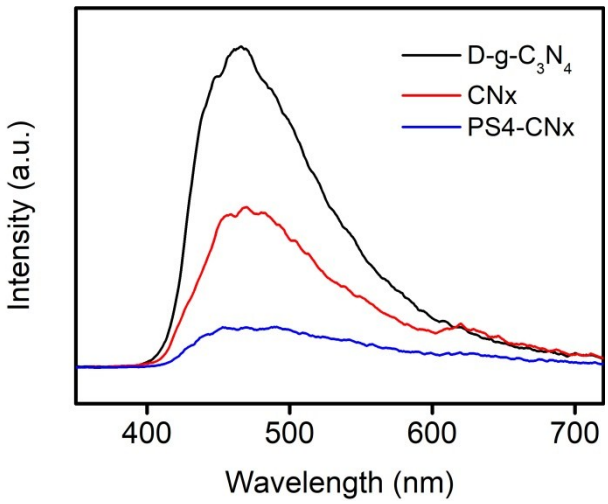

Reference

1. Y. Yuan, Z. Shen, S. Wu, Y. Su, L. Pei, Z. Ji, M. Ding, W. Bai, Y. Chen, Z. Yu and Z. Zou, *Appl. Catal. B: Environ.*, 2019, **246**, 120-128.
2. L. Lin, H. Ou, Y. Zhang and X. Wang, *ACS Catal.*, 2016, **6**, 3921-3931.
3. G. Zhang, L. Lin, G. Li, Y. Zhang, A. Savateer, S. Zafeuratos, X. Wang, and M. Antonietti, *Angew. Chem. Int. Ed.*, 2018, **57**, 9372-9376.
4. A. Ahmed, P. John, M. H. Nawaz, A. Hayat and M. Nasir, *ACS Appl. Nano. Mater.*, 2019, **2**, 5156-5168.
5. Y. Fan, W. Zhang, Y. Liu, Z. Zeng, X. Quan and H. Zhao, *ACS Appl. Mater. Interfaces*, 2019, **11**, 17467-17474.
6. P. Hu, C. Chen, R. Zeng, J. Xiang, Y. Huang, D. Hou, Q. Li and Y. Huang, *Nano Energy*, 2018, **50**, 376-382.
7. L. Zhang, F. Mao, L. R. Zheng, H. F. Wang, X. H. Yang and H. G. Yang, *ACS Catal.*, 2018, **8**, 11035-11041.
8. J. Liu, Z. Wei, W. Fang, Z. Jiang and W. Shangguan, *ChemCatChem*, 2019, **11**, 6275-6281.
9. C. Ye, J. Li, Z. Li, X. Fan, L. Zhang, B. Chen, C. Tung and L. Wu, *ACS Catal.*, 2015, **5**, 6973-6979.
10. S. Huang, X. Kou, D. He, C. Du, X. Wang and Y. Su, *ChemCatChem*, 2019, **11**, 6316-6323.
11. S. Huang, C. Wang, H. Sun, X. Wang and Y. Su, *Nanoscale Res. Lett.*, 2018, **13**, 161.

12. J. Fu, B. Zhu, C. Jiang, B. Cheng, W. You and J. Yu, *Small*, 2017, **13**, 1603938.

13. F. He, G. Chen, J. Miao, Z. Wang, D. Su, S. Liu, W. Cai, L. Zhang, S. Hao and B. Liu, *ACS Energy Lett.*, 2016, **1**, 969-975.

14. G. Liao, Y. Gong, L. Zhang, H. Gao, G. Yang and B. Fang, *Energy Environ. Sci.*, 2019, **12**, 2080-2147.

15. X. She, J. Wu, J. Zhong, H. Xu, Y. Yang, R. Vajtai, J. Lou, Y. Liu, D. Du, H. Li and P. M. Ajayan, *Nano Energy*, 2016, **27**, 138-146.

16. Q. Han, B. Wang, J. Gao, Z. Cheng, Y. Zhao, Z. Zhang and L. Qu, *ACS Nano*, 2016, **10**, 2745-2751.

17. R. Cao, H. Yang, X. Deng, P. Sun, S. Zhang and X. Xu, *ChemCatChem*, 2018, **10**, 5656-5664.

18. X. Wu, D. Gao, H. Yu and J. Yu, *Nanoscale*, 2019, **11**, 9608-9616.

19. M. Liu, P. Xia, L. Zhang, B. Cheng and J. Yu, *ACS Sustainable Chem. Eng.*, 2018, **6**, 10472-10480.

20. H. He, J. Cao, M. Guo, H. Lin, J. Zhang, Y. Chen and S. Chen, *Appl. Catal. B: Environ.*, 2019, **249**, 246-256.

21. Y. You, S. Wang, K. Xiao, T. Ma, Y. Zhang and H. Huang, *ACS Sustainable Chem. Eng.*, 2018, **6**, 16219-16227.

22. Y. Liu, C. Shen, N. Jiang, Z. Zhao, X. Zhou, S. Zhao and A. Xu, *ACS Catal.*, 2017, **7**, 8228-8234.

23. P. Xia, M. Liu, B. Cheng, J. Yu and L. Zhang, *ACS Sustainable Chem. Eng.*,

2018, **6**, 8945-8953.

24. W. Xing, W. Tu, Z. Han, Y. Hu, Q. Meng and G. Chen, *ACS Energy Lett.*, 2018, **3**, 514-519.

25. Y. Wen, D. Qu, L. An, X. Gao, W. Jiang, D. Wu, D. Yang and Z. Sun, *ACS Sustainable Chem. Eng.*, 2019, **7**, 2343-2349.

26. K. Bhunia, M. Chandra, S. Khilari and D. Pradhan, *ACS Appl. Mater. Interfaces*, 2019, **11**, 478-488.

27. J. Chu, X. Han, Z. Yu, Y. Du, B. Song and P. Xu, *ACS Appl. Mater. Interfaces*, 2018, **10**, 20404-20411.

28. C. Yang, Z. Xue, J. Qin, M. Sawangphruk, S. Rajendran, X. Zhang and R. Liu, *J. Phys. Chem. C*, 2019, **123**, 4795-4804.

29. I. Majeed, U. Manzoor, F. Kanodarwala, M. Nadeem, E. Hussain, H. Ali, A. Badshah, J. Stride and M. Nadeem, *Catal. Sci. Technol.*, 2018, **8**, 1183-1193.

30. T. Su, Z. Hood, M. Naguib, L. Bai, S. Luo, C. Rouleau, I. Ivanov, H. Ji, Z. Qin and Z. Wu, *Nanoscale*, 2019, **11**, 8138-8149.

31. X. Shi, M. Fujitsuka, S. Kim and T. Majima, *Small*, 2018, **14**, 1703277.

32. J. Xu, J. Gao, Y. Qi, C. Wang and L. Wang, *ChemCatChem*, 2018, **10**, 3327-3335.

33. Y. Qi, J. Xu, Y. Fu, C. Wang and L. Wang, *ChemCatChem*, 2019, **11**, 3465-3473.

34. G. Zhang, G. Li, Z. Lan, L. Lin, A. Savateer, T. Heil, S. Zafeuratos, X. Wang, and M. Antonietti, *Angew. Chem. Int. Ed.*, 2017, **56**, 13445-13449.

35. X. Xu, X. She, T. Fei, Y. Song, D. Liu, H. Li, X. Yang, J. Yang, H. Li, L. Song, P. Ajayan and J. Wu, *ACS Nano*, 2019, **13**, 11294-11302.

36. L. Lin, H. Ou, Y. Zhang, X. Wang, *ACS Catal.*, 2016, **6**, 3921-3931.

37. J. Xu, Y. Qi, L. Wang, *Appl. Catal. B: Environ.*, 2019, **246**, 72-81.

38. J. Wang, Y. Lu, Z. Xu, *ACS Sustainable Chem. Eng.*, 2017, **5**, 7260-7267

39. X. Fan, Z. Xing, Z. Shu, L. Zhang, L. Wang, J. Shi, *RSC Adv.*, 2015, **5**, 8323-8328.

40. H. Kim, S. Gim, T. H. Jeon, H. Kim, W. Choi, *ACS Appl. Mater. Interfaces*, 2017, **9**, 40360–40368.

41. J. Tian, L. Zhang, M. Wang, X. Jin, Y. Zhou, J. Liu, J. Shi, *Appl. Catal. B: Environ.*, 2018, **232**, 322-329.

42. J. Yuan, Y. Tang, X. Yi, C. Liu, C. Li, Y. Zeng, S. Luo, *Appl. Catal. B: Environ.*, 2019, **251**, 206-212.